ARTICLE

The effect of phosphating time on the electrocatalytic activity of nickel phosphide nanorod arrays grown on Ni foam

Jiale Xing, Zehua Zou, Kailu Guo, and Cailing Xu[a)]
State Key Laboratory of Applied Organic Chemistry, Key Laboratory of Nonferrous Metal Chemistry and Resources Utilization of Gansu Province, Laboratory of Special Function Materials and Structure Design of the Ministry of Education, College of Chemistry and Chemical Engineering, Lanzhou University, Lanzhou 730000, China

(Received 10 August 2017; accepted 19 September 2017)

Recently, highly active, easy-to-make, and efficient bifunctional electrocatalysts have attracted tremendous attention because of their potential applications in clean energy. Herein, we report a simple, one-step approach for fabricating three-dimensional (3D) Ni–P nanorod arrays by direct phosphorization of commercial nickel foam (Ni foam) with different times. When used as a 3D electrode for oxygen evolution reaction, the obtained Ni–P nanorods with two hours of phosphatization treatment display high activity with an overpotential of 270 mV required to generate a current density of 30 mA/cm^2 and excellent stability in 1.0 M KOH. Additionally, the Ni–P nanorod arrays are also highly active for electrocatalyzing the hydrogen evolution reaction in the alkaline media. As a result, the bifunctional Ni–P catalysts enabled a highly performed overall water splitting, in which a low applied external potential of 1.6 V led to a stabilized catalytic current density of 10 mA/cm^2 over 12 h.

I. INTRODUCTION

The increasing global energy demand and accompanying climate changes as well as environmental issues are driving scientists to search for sustainable and environmentally friendly alternative sources of energy to replace exhaustible fossil fuels.[1] Hydrogen has been considered as an efficient and clean energy resource to replace the depleting fossil fuel in the 21st century.[2,3] Recently, the electrocatalytic water splitting for generating hydrogen and oxygen has attracted extensive attentions because this process provides a promising approach for the production of a sustainable, secure, and clean hydrogen-fuel energy.[4–6] This electricity-driven process can be divided into two half-reactions, namely, the four-electron oxygen evolution reaction (OER) and the two-electron hydrogen evolution reaction (HER).[7,8] Thereinto, the OER is thermodynamically and kinetically sluggish due to the four proton-coupled electron transfer process.[9] Thus, it still remains a great challenge to develop the efficient and high-active bifunctional electrocatalysts for overall water splitting. Currently, the state-of-the-art electrocatalysts are the precious metal and their composites such as Pt, RuO_2, and IrO_2.[10,11] However, the high cost and limited availability of noble metals potentially obstruct their large-scale applications in overall water splitting. In this case, tremendous research efforts have been focused on the low-cost and earth-abundant catalysts as alternatives to the noble metal. For example, Yang's group reported the iron-nickel sulfide (INS) ultrathin nanosheets (NSs) that enabled a catalytic current density of 10 mA/cm^2, an even lower overpotential of 105 mV at 10 mA/cm^2, and a smaller Tafel slope of 40 mV/dec for HER.[12] Also, Sun's group synthesized new hierarchically multifunctional porous nickel sulfide superstructures (h-NiS_x) through electrodeposition of porous metallic Ni microsphere arrays on a nickel foam followed by low-temperature sulfurization.[13] The h-NiS_x exhibited outstanding catalytic performance for both HER and OER in an alkaline electrolyte (1.0 M KOH), in which the overpotentials of h-NiS_x to afford a current density of 10 mA/cm^2 are as small as 60 mV for HER and 180 mV for OER in 1.0 M KOH, respectively.[13] Except for the transition metal sulfides,[12,13] transition metal selenides,[14,15] carbides,[16,17] borides,[18] nitrides,[19,20] and phosphides[21–26] have also been extensively studied in recent years. A series of magnetic iron-doped molybdenum carbide ($Mo_{2-x}Fe_xC$) nanomaterials were synthesized by Wan et al. for the first time and enhanced catalytic activities for HER were obtained.[17] Also, Hu et al. fabricated Co–N–mC catalysts in which two forms of metals including coordinating Co moieties and Co nanoparticles (CoNPs) were encapsulated in mesoporous N-doped carbon hollow spheres (Co–N–mC).[20] The obtained Co–N–mC showed excellent catalytic performance for the oxygen reduction reaction.

Among them, transition metal phosphides such as Ni–P,[21–23] Co–P,[24–26] Fe–P,[27] Mo–P,[28] and W–P,[29] have drawn intense attention because of their good

Contributing Editor: Yao Zheng
[a)]Address all correspondence to this author.
e-mail: xucl@lzu.edu.cn, xucl921chem@163.com
DOI: 10.1557/jmr.2017.399

electrocatalytic performance for overall water splitting. Especially, nickel phosphide is considered as the most promising prospect due to the excellent electrocatalytic performance toward HER and OER.[21–23] To achieve high catalytic activity, numerous nickel phosphide nanomaterials with various micro/nanostructures like nanowires, NSs, nanoparticles, and nanonflowers were prepared by different methods such as high-temperature wet chemical processes,[30] hydrothermal methods,[31] electrochemical deposition,[32] and phosphidation of nanostructured nickel oxide/hydroxides.[22,33] Li et al. reported the bifunctional Ni_xP_y-325 catalysts that enabled a catalytic current density of 10 mA/cm^2 at 1.57 V in the alkaline media for overall water splitting.[34] Afterward, Stern et al. synthesized Janus Ni_2P catalysts that achieved a current density of 10 mA/cm^2 toward overall water splitting at 1.63 V in the alkaline electrolyte. Liu et al. synthesized the Ni–P nanoparticles that can achieve a current density of 10 mA/cm^2 at 1.68 V in the alkaline media for overall water splitting.[33] Recently, the direct phosphorization of nickel foam to fabricate 3D nickel phosphide nanostructures has been found to perform high electrocatalytic activities for hydrogen production.[23,35] For example, Wang et al. reported a one-step route to the synthesis of an integrated nickel phosphide nanorods/nickel (Ni_2P-NRs/Ni) electrode by direct phosphorization of commercially available Ni foam under solvothermal conditions using red phosphorus as the precursor, showing better electrochemical performance for HER.[23] Also, Liu's group reported a very simple and straight forward method to fabricate self-supported biphasic Ni_5P_4–Ni_2P NS arrays for HER by direct phosphorization of the Ni foam using phosphorus vapor without complicated chemical reactions and post treatment steps involved.[35] Additionally, three-dimensional (3D) porous Ni/Ni_8P_3 electrodes and $Ni_{12}P_5$/Ni_2P nanowires were prepared by phosphorization of commercial Ni foam, respectively, for the overall water splitting.[36,37] Despite this significant progress, they still suffered from the large overpotential for oxygen production, which lead to the high cell voltage of water electrolysis. Therefore, the development of alternative bifunctional electrocatalysts with low overpotential and long-term stability is highly desirable and challenging.

To obtain the optimal catalyst for overall water splitting, a variety of reaction conditions have been changed in the synthesis of transition metal phosphide, such as changing the reaction time and temperature or changing the quantity of phosphorus source.[22,25,38] For example, You et al. synthesized a series of Co–P/NC under different phosphidation times and achieved the best HER and OER activity at 2 h.[38] Although there have been many reports focused on the method of direct phosphorization of the nickel foam to synthesis nickel phosphide, only few have studied the effect of phosphating time on the performance of HER and OER when NaH_2PO_2 is used as the phosphorus source. Therefore, we tested the effects of phosphating time on their electrocatalytic activities toward HER and OER in the alkaline media.

Herein, we synthesized the biphasic $Ni_{12}P_5$–Ni_2P nanorod arrays by direct phosphorization of commercial nickel foam (Ni foam) with different phosphating times. The method requires neither a special nickel precursor nor a surface-active agent added but to achieve well-dispersed Ni–P nanorod arrays that are directly grown on the Ni foam surface. The effects of phosphating time on their electrocatalytic activities toward HER and OER were investigated in the alkaline media. The results show that the phosphating time plays a crucial role to the electrocatalytic activities for OER and HER. The as-prepared Ni–P nanorods with two hours of phosphating treatment display an overpotential of 270 mV to generate a current density of 30 mA/cm^2 for OER and an overpotential of 158 mV to deliver a current density of 10 mA/cm^2 for HER as well as excellent stability in 1.0 M KOH, which demonstrate that the as-prepared self-supported Ni–P nanorod array electrode can be directly used either as a cathode to drive HER or as an anode to expedite OER without any post treatment. As a result, a cell voltage as low as 1.6 V is needed to drive a current density of 10 mA/cm^2 for overall water splitting, when the Ni–P nanorods are used as a bifunctional electrode for basic water splitting. Moreover, Ni–P nanorods possess high efficiency and long-term stability, indicating a low-cost and high-performance electrocatalyst for full water splitting.

II. EXPERIMENTAL SECTIONS

A. Materials

Nickel foam with a thickness of 1.6 mm and a pore density of 110 ppi was purchased from Changsha Keliyuan Instruments Co., Ltd. (Changsha, China). Sodium hypophosphite ($NaH_2PO_2·H_2O$), HCl (37.5%) and acetone (99.5%) were all of analytical grade and used as purchased without further purification. Iridium(IV) dioxide (IrO_2) was purchased from Alfa Aesar (Haverhill, Massachusetts). Carbon-supported Pt nanoparticles (Pt/C, 20 wt% Pt) were supplied by Johnson Matthey Inc. (New York, New York). Nafion (5% in a mixture of lower aliphatic alcohols and water) was purchased from Sigma-Aldrich (St. Louis, Missouri). Ultrapure water (18.2 MΩ/cm) supplied with an Aike water system was used for solution preparation.

B. Preparation of Ni–P nanorod arrays on Ni foam

Caution: Because this procedure involves the high-temperature decomposition of sodium hypophosphite that can liberate phosphine, this reaction should be considered as highly corrosive and flammable and therefore should

only be carried out by a person who is trained appropriately under rigorous air-free conditions.

Ni–P nanorod arrays were prepared according to the reference with minimal changes.[39] Firstly, the Ni foam (1 × 2 cm) was completely immersed in an ultrasound bath of acetone, 3 M HCl, ethanol, and DI water, respectively, for 15 min to well clean the surface of the Ni foam and then dried at room temperature. Secondly, the treated Ni foam was loaded on the top of the ceramic boat with 0.3 g $NaH_2PO_2{\cdot}H_2O$ powder at the bottom. And then the furnace was heated up to 300 °C with a heating rate of 1 °C/min under a flow of N_2 atmosphere and kept at 300 °C for different times, such as 1, 2, and 3 h. After cooling down to room temperature, the samples were taken out and rinsed several times with DI water and ethanol, respectively, and then dried under vacuum at 60 °C. The Ni–P nanorod samples prepared with different phosphating times were denoted as Ni–P 1 h, Ni–P 2 h, and Ni–P 3 h, respectively.

C. Material characterizations

Powder X-ray diffraction (XRD) patterns were obtained by a Rigaku D/Max-2400 diffractometer with Cu K_α irradiation (λ = 1.5406 Å) at a scanning rate of 5°/min from 10 to 80° to characterize the crystal structure of the samples. The morphology and microstructure of the samples were investigated by field emission scanning electron microscopy (FESEM; JEOLJSM-S4800, JEOL Ltd., Tokyo, Japan; operating voltage, 5 kV) and transmission electron microscopy (TEM; TecnaiTM G2F30, FEI, Hillsboro, Oregon; operated at 200 kV) with energy dispersive spectroscopy EDX and selected area electron diffraction SAED. X-ray photoelectron spectroscopy (XPS) measurements were recorded by using a VGES-CALBMKII X-ray photoelectron spectrometer (VG Instruments, Middlewich, United Kingdom) with monochromated Al K_α radiation (1486.6 eV).

D. Electrochemical measurements

The HER and OER properties were recorded at room temperature on a CHI 760E electrochemical workstation with a three-electrode system, equipped with a Hg/HgO reference electrode and a Pt plate (2 × 2 cm) counter electrode. The as-prepared Ni–P nanorod arrays on the Ni foam were directly used as the working electrode. Cyclic voltammetry was carried out at a scan rate of 5 mV/s to activate the as-fabricated electrodes. The polarization curves for HER and OER were recorded by a linear sweep of potential from −0.8 to −1.5 and 0 V–0.8 V (versus Hg/HgO) with a sweep rate of 5 mV/s, respectively. Electrochemical impedance spectroscopy (EIS) was tested in the frequency range from 10^5 to 10^{-2} Hz at open circuit potential at room temperature. For overall water splitting tests, the obtained Ni–P nanorod electrodes were used as negative and positive electrodes for HER and OER, respectively. The CV curve was obtained from 0 to 2 V at a scan rate of 5 mV/s. All the polarization curves were recorded with 95% iR compensation. IrO_2 and 20 wt% Pt/C was loaded on the nickel foam with 2.5 mg/cm^2 for the comparative experiments. The working electrodes of IrO_2 and 20 wt% Pt/C were prepared as follows: a homogeneous suspension was firstly prepared by ultrasonically mixing 2.5 mg of IrO_2 or 20 wt% Pt/C with 50 μL of Na^+-exchanged Nafion solution and 950 μL of isopropanol solvent for 30 min. Then, 1 mL of the prepared catalytic suspension was loaded onto the surface of an Ni foam (1 × 1 cm) using a micropipette. Finally, the electrode was allowed to dry overnight under atmosphere at room temperature to form a thin catalyst film on the Ni foam. The electrolyte in all the experiments was 1.0 M KOH aqueous solution.

III. RESULTS AND DISCUSSION

A. Composition, structure and morphology

Sodium hypophosphite (NaH_2PO_2) has been proven to be an effective phosphorus source to prepare specific phosphides.[22,23,34,40] The biphasic Ni–P nanorods were grown on the acid-treated Ni Foam via direct phosphorization of the Ni foam in a tube furnace, where $NaH_2PO_2{\cdot}H_2O$ provided the phosphorous vapor. In this process, the Ni foam turned black but maintains its three-dimensional structure. Thus, it can be directly used as an electrode for HER and OER without any post processing steps. Furthermore, the Ni–P electrode showed high flexibility, which was beneficial for being used as a water splitting electrode. To inspect the surface morphologies of the self-supported Ni–P electrodes, FESEM was first carried out, and the FESEM images of the samples with different phosphorization times are shown in Fig. 1. Figure 1(a) shows the smooth surface of the acid-treated Ni foam with some visible pores. As shown in Figs. 1(b)–1(d), numerous nanorods with diameters of ~500 nm were lushly grown on the surface of the Ni foam after direct phophorization of the Ni foam, and the nanorods displayed a rough surface composed of the tiny fibers, which can provide high specific surface area for the outstanding electrochemical properties. From Figs. 1(b)–1(d), it can be also concluded that the phosphorization time had an unconspicuous influence on the surface morphologies of the samples.

The XRD was then executed to detect the crystal texture of the obtained Ni–P electrode at different phosphorization times. As shown in Fig. 2(A), hexagonal $Ni_{12}P_5$ (JCPDS No. 74-1381)[41] and Ni_2P (JCPDS No. 74-1385)[42] can be clearly found from the Ni–P samples obtained by direct phosphotization of the Ni foam, except for the metallic Ni phase. The diffraction peaks located at 40.7°, 44.8°, 47.4°, 54.2°, and 74.8° can be indexed to the (111), (201), (210), (300), and (212) planes of the cubic phase Ni_2P (JCPDS

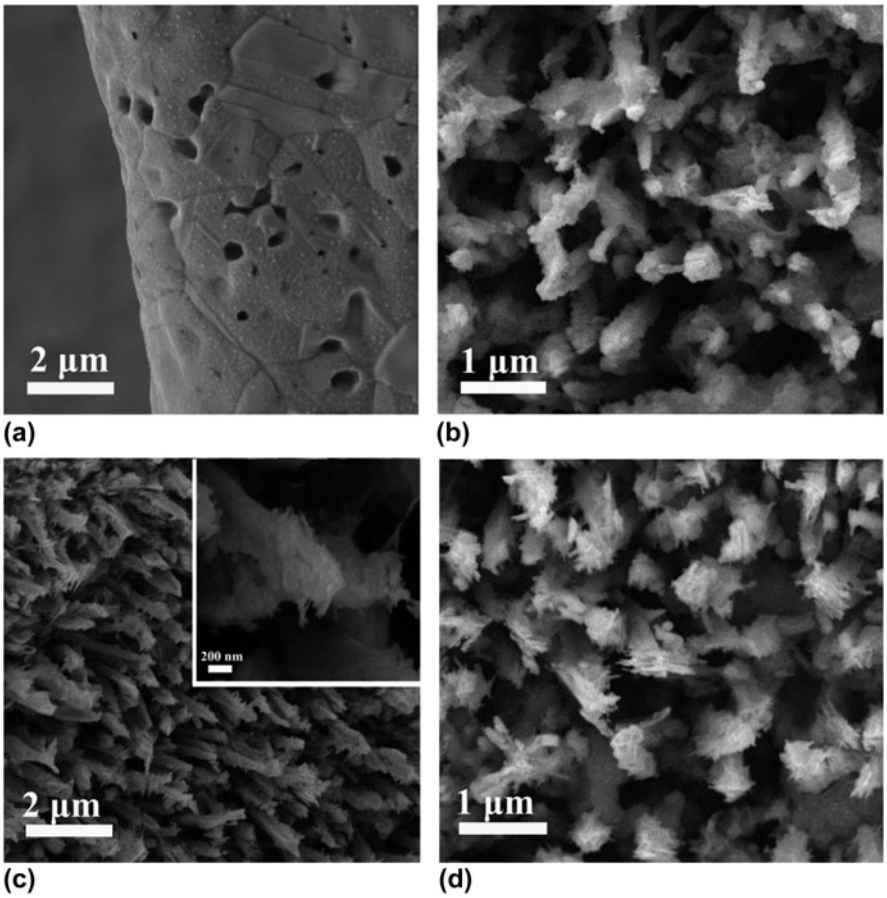

FIG. 1. FESEM of (a) Ni foam and the Ni–P samples with different phosphating treatments for (b) 1 h, (c) 2 h, and (d) 3 h.

No. 74-1385),[42] while the peaks at 38.4°, 41.7°, 47.4°, and 48.9° correspond to the (112), (400), (201), and (312) planes of $Ni_{12}P_5$ (JCPDS No. 74-1381).[41] In addition, the strong peaks at 44.5°, 52.0°, and 76.5° can be assigned to the metal Ni, which is from the Ni substrate. Moreover, the phosphorization time has an unconspicuous influence on the dominate phase of the samples. The mass loading of Ni–P samples with a phosphating treatment of two hours is averaged and calculated to be in the range of 2.37 (Ni_2P)–2.74 ($Ni_{12}P_5$) mg/cm^2, according to the molar of P and the results of XRD.

Moreover, the surface chemistry states of the Ni–P sample with a phosphating treatment of two hours were investigated by XPS due to the preferable electrochemical performance. The XPS survey spectra clearly proved the presence of Ni and P in the Ni–P sample [Fig. 2(B)].[32] The high-resolution spectrum of Ni 2*p* [Fig. 2(C)] clearly shows two spin–orbit doublets of Ni $2p_{3/2}$ and Ni $2p_{1/2}$ and two shake-up satellites (identified as "sat.") at 860.1 eV and 878.8 eV, respectively.[32,43] The peaks [Fig. 2(C)] at 852.8 and 869.5 eV can be assigned to the metal Ni which originated from the Ni substrate, and the peaks at 855.3 and 873.7 eV are corresponding to the oxidized Ni species in the Ni–P sample.[32,35] Figure 2(D) shows the XPS spectrum of P 2*p*, which can also be split into two peaks at binding energies of 129.4 and 130.0 eV, corresponding to P $2p_{3/2}$ and P $2p_{1/2}$, and the other peak centered at 133.1 eV, which is assigned to the oxidized phosphorus species, such as PO_4^{3-} or P_2O_5,[22,32,33] arises from the inescapable contact between the Ni–P surface and air. These results confirm the direct formation of nickel phosphate on the Ni foam without using extra nickel precursors.[22,32,33]

To further study the microstructure and chemical composition of the nanorods, TEM of the Ni–P sample with a phosphating treatment for two hours was also carried out and shown in Fig. 3. The Ni–P nanorod shows a cone-like morphology with a length of about 4 μm and a diameter of about 500 nm [Fig. 3(a)]. The HRTEM exhibits well-defined lattice fringes of an adjacent space of 0.218 nm, confirming the (111) plane of the hexagonal Ni_2P,[43,44] as shown in Fig. 3(b). The chemical compositions of Ni–P were measured by elemental mapping, verifying the homogeneous distribution of Ni and P elements across the nanorod structure [Figs. 3(c)–3(e)]. All of the results clearly confirm the successful growth of nickel phosphide nanorod arrays on the Ni foam after direct phosphorization treatment of the Ni foam.

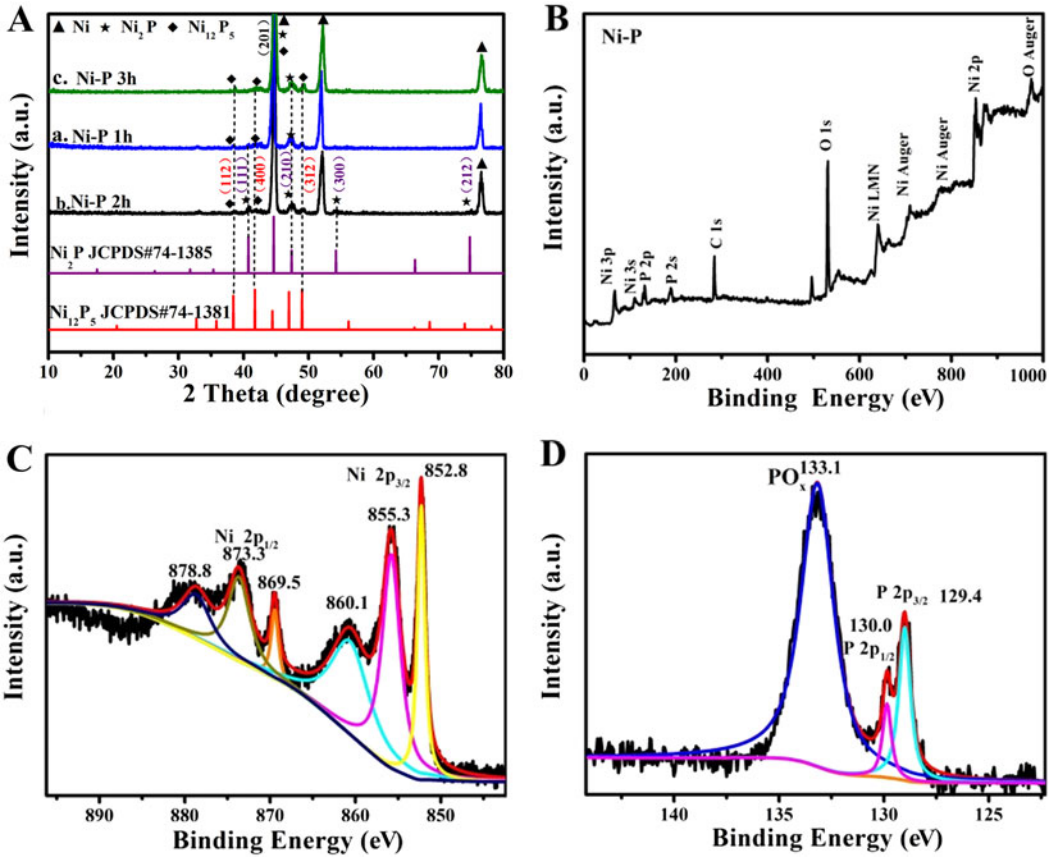

FIG. 2. (A) XRD patterns of the Ni–P samples with phosphating treatment for (a) 1 h, (b) 2 h, and (c) 3 h. (B) XPS survey spectrum and high-resolution spectra of Ni 2*p* (C) and P 2*p* (D) for the Ni–P sample with 2 h phosphating treatment.

B. Electrocatalytic properties toward HER and OER

Electrocatalytic properties of the Ni–P nanorods were evaluated using a typical three-electrode setup. Firstly, we investigated the effect of reaction time on the electrocatalytic activity for HER and OER in 1 M KOH solution, respectively, as shown in Figs. 4 and 5. The linear sweep voltammograms (LSVs) of HER in Fig. 4(A) reveal that the Ni–P samples possess a much lower onset overpotential and higher current density than those of bare Ni foam. When the phosphorization time is two hours, the electrocatalytic activity of the Ni–P sample for HER attains the highest level. It only needs an overpotential of 158 mV to drive the current densities of 10 mA/cm^2, which is comparable to those of many reported Ni-phosphide-based electrocatalysts in the alkaline media (see Table I). Increasing or decreasing the reaction time would induce a decreased activity for Ni–P, suggesting a phosphating time-depended HER catalytic activity for the Ni–P catalysts. Figure 4(B) presents the Tafel plots of the Ni foam, Pt/C, and the Ni–P samples with different phosphating times. These Tafel plots are fitted to the Tafel equation ($\eta = b \log [j] + a$, where j is the current density and b is the Tafel slope).[23,45] The Tafel slope of 38 mV/dec for Pt/C is consistent with the value reported in the literature.[30,46] The Ni–P exhibits a Tafel slope of 75 mV/dec, which is larger than that of Pt/C (38 mV/dec) but lower than that of the Ni foam (108 mV/dec) and superior to that of many earth-abundant HER catalysts reported recently, such as Ni–P nanoparticles (87 mV/dec at η = 60–140 mV, 81 mV/dec at η = 150–200 mV),[46] Ni_2P (87 mV/dec)[30] and different Mo_2C nanocrystals (110–235 mV/dec).[47] Benefiting from the lower Tafel slope, the smaller overpotential is required to achieve the same cathodic current density, suggesting a faster HER response for Ni–P electrode. Additionally, according to the previous report,[37,48] the Tafel slope of 75 mV/dec shows a combined Volmer ($H_2O + e^- \rightarrow H_{ads} + OH^-$)–Heyrovsky ($H_{ads} + H_2O + e^- \rightarrow H_2 + OH^-$) mechanism for HER in the alkaline media. Such a pathway includes the adsorption of H_2O and the electrochemical decomposition of trapped H_2O into the adsorbed H atoms (H_{ads}) and OH^- species and then the detachment of OH^- to refresh the surface and the formation of H_{ads} to yield H_2.

Compared to HER, OER, the anodic reaction of water splitting, is usually more difficult to accomplish, as it is a thermodynamically and kinetically demanding process

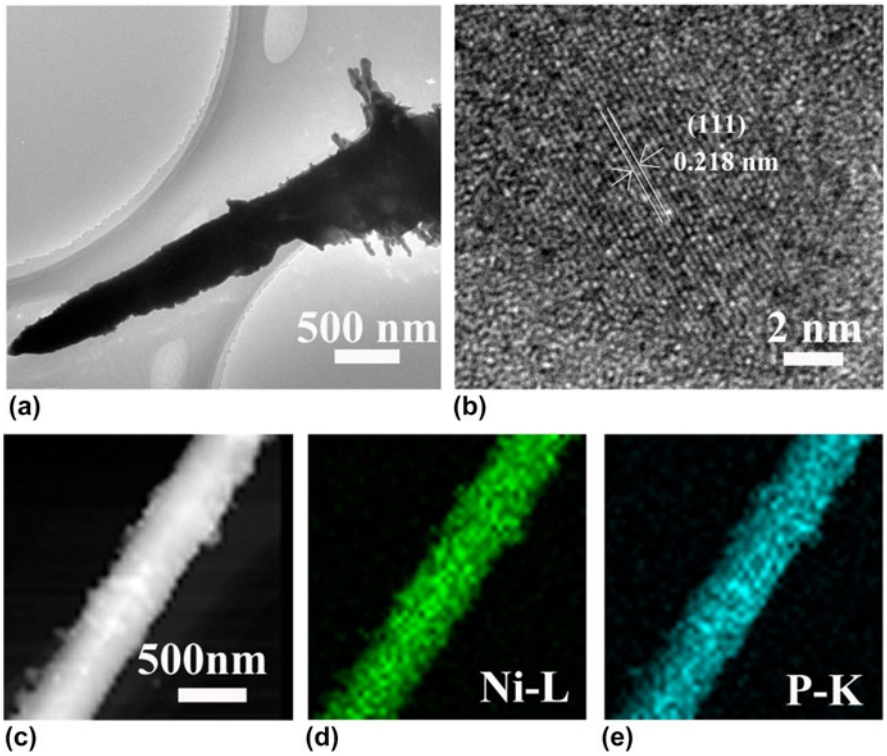

FIG. 3. TEM (a), HRTEM (b), STEM (c), and the elemental mapping (d, e) images of the Ni–P sample with 2 h of phosphating treatment.

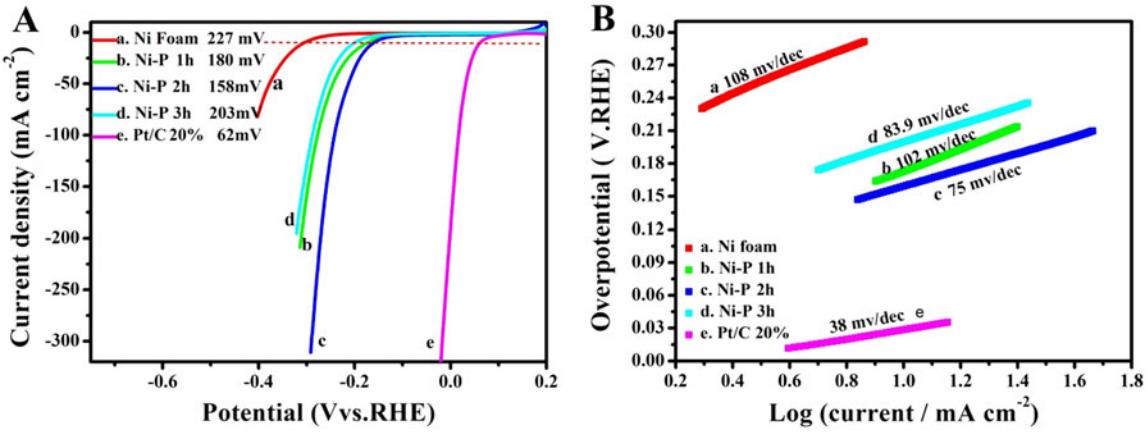

FIG. 4. The LSVs (A) and the corresponding Tafel plots (B) of Ni foam (a), Pt/C (e) and the Ni–P samples with phosphating treatment for (b) 1 h, (c) 2 h, and (d) 3 h for HER.

involving four sequential proton-coupled charge transfer steps and the O=O bond formation. The Ni–P samples also show superior electrochemical activity toward OER. Figure 5 is the LSVs and the corresponding Tafel plots for OER. Note that the polarization curves of Ni–P samples have an obviously oxidative peak at 1.4 V versus RHE, which is ascribed to the oxidation of Ni species.[33] After that, it begins for OER.[33] The current density of oxidative peaks is about 20 mA/cm^2. Therefore, to eliminate the effect of the anodic peak current of Ni species, the overpotential at a current density of 30 mA/cm^2 is used to certify the electrochemical activity of Ni–P samples. At the current density of 30 mA/cm^2, the Ni–P sample with phosphating treatment for two hours shows the smallest overpotential of 270 mV, compared to other samples including the Ni foam, the commercial benchmark OER catalyst IrO_2. Additionally, it is superior to or comparable with the behavior of other Ni-phosphide-based electrocatalysts (as show in Table I) and other transition metal phosphide in the alkaline media, such as Ni_xP_y (340 mV for 10 mA/cm^2),[37] Ni_2P (290 mV for 10 mA/cm^2),[33] Co–P (319 mV for

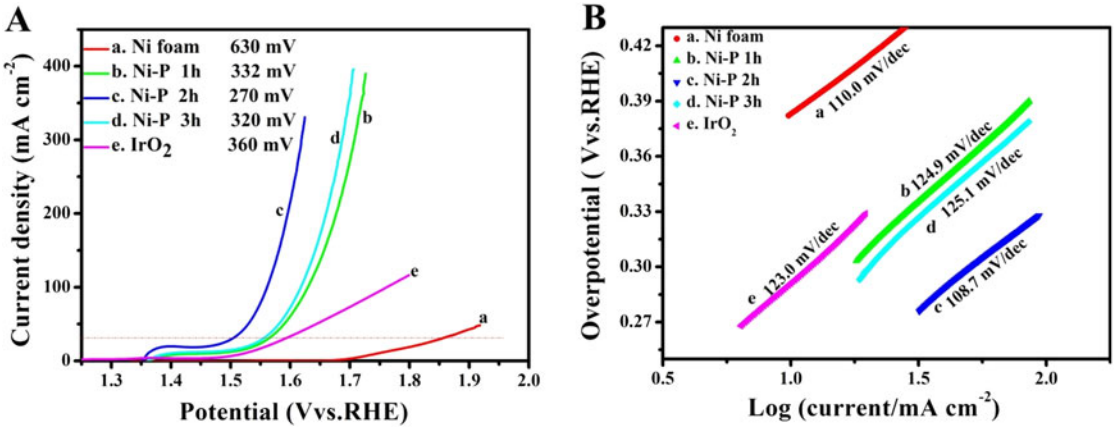

FIG. 5. The LSVs (A) and the corresponding Tafel plots (B) of Ni foam (a), IrO_2 (e) and the Ni–P samples with phosphating treatment for (b) 1 h, (c) 2 h, and (d) 3 h for OER.

TABLE I. Overpotential and Tafel slope of the reported Ni-phosphide-based electrocatalysts for OER and HER in 1 M KOH.

Catalyst	Electrolyte	Water electrolysis test	Overpotential (mV)	Tafel slope (mV/dec)	Reference
Ni_xP_y	1 M KOH	OER	340 mV at 10 mA/cm^2	72.2	*ACS Appl. Mater.* **8**(17), 10826–10834 (2016)
		HER	160 mV at 20 mA/cm^2	107.3	
Ni/Ni_8P_3	1 M KOH	OER	230 mV at 10 mA/cm^2	73.2	*Adv. Funct. Mater.* **26**(19), 3314–3323 (2016)
		HER	130 mV at 10 mA/cm^2	58.5	
Ni–P	1 M KOH	OER	220 mV at 10 mA/cm^2	120	*J. Power Sources.* **299**, 342–346 (2015)
		HER	98 mV at 10 mA/cm^2	55	
Ni_2P	1 M KOH	OER	290 mV at 10 mA/cm^2	47	*Energy Environ. Sci.* **8**(8), 2347–2351 (2015)
		HER	221 mV at 10 mA/cm^2	...	
C@ Ni_8P_3	1 M KOH	OER	267 mV at 10 mA/cm^2	64	*ACS Appl. Mater.* **8**, 27850–27858 (2016)
		HER	144 mV at 10 mA/cm^2	59	
Ni–P nanoplates	1 M KOH	OER	300 mV at 10 mA/cm^2	64	*Energy Environ. Sci.* **9**, 1246–1251 (2016)
		HER	110 mV at 10 mA/cm^2	73	
Ni–P NA/NF	1 M KOH	OER	311 mV at 20 mA/cm^2	76	*RSC Adv.* **6**, 107859–107864 (2016)
		HER	148 mV at 10 mA/cm^2	115.2	
Ni–P	1 M KOH	**OER**	**270 mV at 30 mA/cm^2**	**122**	**This work**
		HER	**158 mV at 10 mA/cm^2**	**75**	

10 mA/cm^2),[38] CoMnP (330 mV for 10 mA/cm^2),[9] CoP (320 mV for 10 mA/cm^2),[7] CoP hollow polyhedron (400 mV for 10 mA/cm^2),[49] Ni–P/C (300 mV for 10 mA/cm^2),[48] and other non-precious metal-based electrocatalysts, such as amorphous NiO (470 mV for 10 mA/cm^2),[50] $NiCo_2O_4$ (391 mV for 10 mA/cm^2),[51] Ni/Ni_3N foam (399 mV for 10 mA/cm^2),[52] NiCo LDH (393 mV for 10 mA/cm^2),[53] and Ni–Co–O@NiCo–S NA (286 mV for 10 mA/cm^2)[54] and is even comparable with the behavior of IrO_2 (340 mV)[55] in 1.0 M KOH. The OER kinetics of the Ni–P electrode is also estimated by corresponding Tafel plots [Fig. 5(B)]. A high-performance electrocatalyst with lower overpotential requires less energy to achieve the same current density. Compared to the HER, the OER is usually more difficult to accomplish, as it is a thermodynamically and kinetically demanding process involving four sequential proton-coupled charge transfer steps and the O=O bond formation. The advantage of the Ni–P electrode on OER is significant for an electrode when used as water splitting. The OER kinetics is also estimated by corresponding Tafel plots [Fig. 5(B)] for these electrodes. The Tafel slope for Ni–P is 106 mV/dec, which is smaller than that of the Ni Foam (110 mV/dec), IrO_2 (123 mV/dec), Ni–P 1 h (124.9 mV/dec), and Ni–P 3 h (125.1 mV/dec), implying a more rapid OER rate for the Ni–P electrode.

To investigate the internal character of all the electrode materials, the exchange current density (j_0) was calculated using extrapolation methods.[45,56] Exchange current density is the intrinsic property of the electrode reaction, which depends only on catalyst materials, electrolyte, and temperature.[1] It reflects the ability of electron transfer and the difficulty of an electrode reaction. The internal reason of overpotential is the exchange current density.[45,56] Electrode reactions with a larger exchange current density need less driving force (smaller current density) to conduct the reaction. The intersection of the extrapolated linear part of the Tafel plots and the X-axis is the

exchange current density.[1] For HER, when the overpotential value is 0, the log[j] values for the Ni foam, Ni–P 1 h, Ni–P 2 h Ni–P 3 h, and Pt/C are −1.9, −1.1, −0.7, −1.4, and 0.33, respectively. Based on Tafel equations ($\eta = b \log[j] + a$, where j is the current density and b is the Tafel slope), j_0 for the Ni foam, Ni–P 1 h, Ni–P 2 h, Ni–P 3 h, and Pt/C were calculated to be 0.013, 0.078, 0.204, 0.035, and 2.18 mA/cm^2, respectively. Moreover, for OER, the log[j] values for the Ni foam, Ni–P 1 h, Ni–P 2 h Ni–P 3 h and IrO_2 are −2.46, −1.18, −1.055, −1.10, and −1.36, respectively. j_0 for the Ni foam, Ni–P 1 h, Ni–P 2 h Ni–P 3 h, and Pt/C were calculated to be 0.003, 0.066, 0.088, 0.079, and 0.043 mA/cm^2, respectively. For both HER and OER, the Ni–P 2 h electrode possess the maximum exchange current density compared to the Ni foam, Ni–P 1 h, and Ni–P 3 h, which proves that the Ni–P 2 h electrode is the optimal catalyst for HER and OER.

The above results demonstrate the desired electrocatalytic activity of the Ni–P nanorods prepared by two hours of phosphorization of the Ni foam, which could be caused by the difference in the number of active sites and the charge transfer capacity of the active materials. The relative electrochemical active surface (ECSA) is

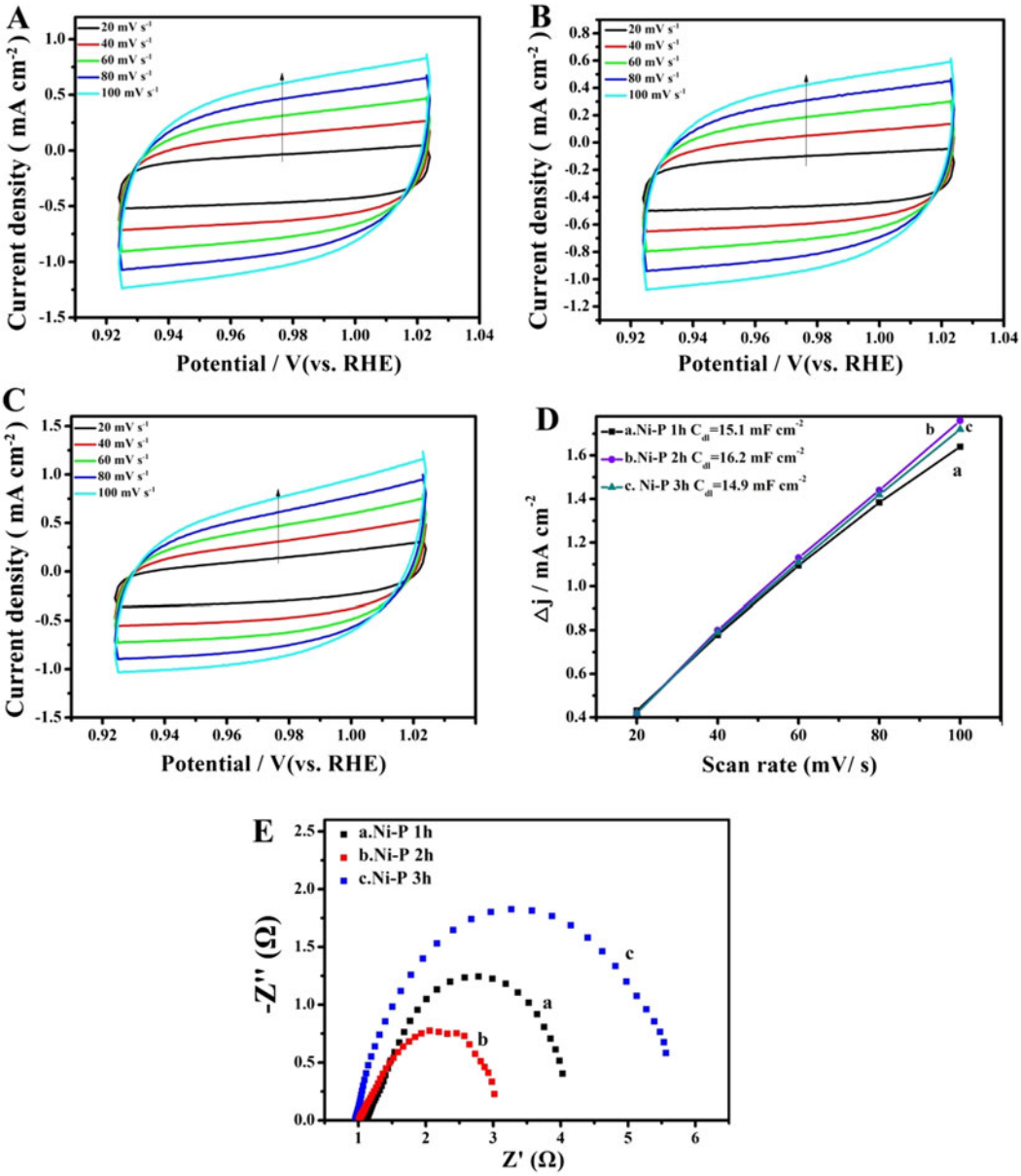

FIG. 6. CV curves between 0.92 and 1.02 V of the Ni–P samples with phosphating treatment for (A) 1 h, (B) 2 h, and (C) 3 h at different scan rates; (D) Plots of the current density versus scan rates derived from CV curves and (E) EIS of the Ni–P samples with phosphating treatment for (a) 1 h, (b) 2 h, and (c) 3 h.

proportional to the number of electrochemically active sites. An efficient method to estimate the ECSA is to test the electrochemical double-layer capacitance (C_{dl}), which is assumed to be linearly proportional to the ECSA (ECSA = C_{dl}/C_s, C_s is specific capacitance).[57,58] The CV curves were swept in the potential range of 0.92–1.02 V versus RHE at various scan rates (20, 40, 60, 80, 100 mV/s) and shown in Figs. 6(A)–6(C). From Fig. 6(D), the C_{dl} can be calculated to be 15.1 mF/cm^2, 16.2 mF/cm^2, and 14.9 mF/cm^2 for Ni–P 1 h, Ni–P 2 h, and Ni–P 3 h, respectively. In this study, the value of C_s that we use is 0.040 mF/cm^2, which is based on the previously reported Ni-based OER catalysts.[58] The EASA of Ni–P 2 h can be calculated as 405 cm^2, which is higher than that of Ni–P 1 h (ECSA = 377.5 cm^2) and Ni–P 3 h (ECSA = 372.5 cm^2). These results confirm that the Ni–P 2 h sample possesses the largest active surface area and enhanced active sites among the three samples. Furthermore, the EIS of the as-prepared samples was also used to evaluate the electrocatalytic kinetics

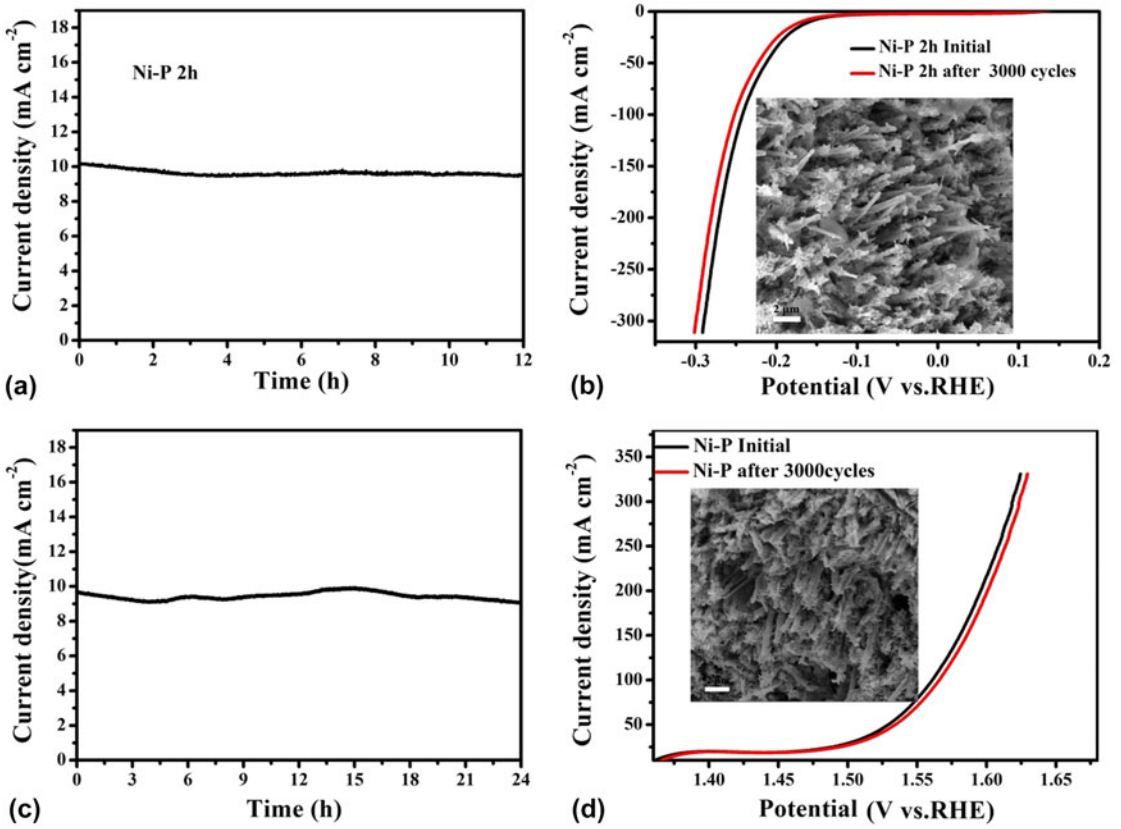

FIG. 7. Chronoamperometric measurements under static overpotential and LSVs recorded before and after 3000 cycles of CV scans for long-term stability tests of the Ni–P sample with two hours of phosphating treatment for HER (a, b) and OER (c, d). Inset: FESEM images of the Ni–P sample after 3000 cycles of CV scans for HER and OER in 1 M KOH solution.

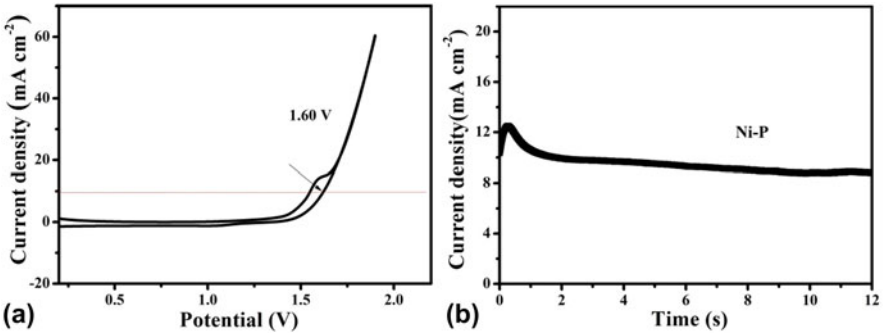

FIG. 8. (a) CV curve and (b) Chronoamperometric curves at 1.6 V of water splitting for the Ni–P sample with 2 h of phosphating treatment in a two-electrode configuration.

TABLE II. The electrocatalytic performance of different nickel phosphide for overall water splitting.

Catalyst	Electrolyte	Cell voltage (V) at 10 mA/cm^2	Reference
C@Ni_8P_3	1 M KOH	1.65	*ACS Appl. Mater. Interfaces* **8**, 27850–27858 (2016)
Ni/Ni_8P_3	1 M KOH	1.56	*Adv. Funct. Mater.* **26**(19), 3314–3323 (2016)
Ni–P	1 M KOH	1.68	*J. Power Sources.* **299**, 342–346 (2015)
Ni_2P	1 M KOH	1.6	*J. Mater. Chem. A* **4**, 5639–5646 (2016)
Ni_2P	1 M KOH	1.49	*ACS Catal.* **6**(2), 714–721 (2016)
Ni–P	1 M KOH	1.69	*RSC Adv.* **6**(109), 107859–107864 (2016)
Ni_xP_y-325	1 M KOH	1.57	*ACS Appl. Mater. Interfaces* **8**(17), 10826–10834 (2016)
CP@Ni–P	1 M KOH	1.63	*Adv. Funct. Mater.* **26**(23), 4067–4077 (2016)
Ni–P	1 M KOH	1.65	*ChemCatChem* **8**(1), 106–112 (2016)
Ni–P	**1 M KOH**	**1.60**	**This work**

during the electrochemical process. The Nyquist plots [Fig. 6(E)], which were tested at the same applied voltage, show that the Ni–P 2 h sample has the smallest charge transfer resistance compared with the Ni–P 1 h and Ni–P 3 h samples, promoting electron charge transfer and offering faster electrochemical kinetics.[37]

Durability and stability in high concentration alkaline solutions are important parameters to evaluate the performance of catalysts in practical applications. Therefore, the electrocatalytic stability of the Ni–P sample with two hours of phosphating treatment toward HER and OER was also investigated using chronoamperometry at a constant overpentional of 158 mV for HER and 270 mV for OER in 1 M KOH, respectively. As shown in Figs. 7(a) and 7(c), a stable current density of about 10 mA/cm^2 for over 24 h of continuous operation was obtained at a constant overpentional of 158 mV for HER. While the sample shows a slightly lower current density than 30 mA/cm^2 at a constant overpentional of 270 mV for OER, the degradation of the current density is negligible after a long period of 24 h. The favorable stability of the Ni–P nanorods was also certified from long-term potential cycling by taking continuous CV scans at 10 mV/s for 3000 cycles. The LSVs are recorded before and after 3000 cycles are displayed in Figs. 7(b) and 7(d). Upon 3000 continuous CV cycles at 10 mV/s, the polarization curves for HER and OER show a slight decay with an overpotential increase of about 8.6 mV and 5.5 mV at 10 mA/cm^2 and 30 mA/cm^2, respectively, compared with the initial one. In addition, the FESEM images of the Ni–P sample after 3000 CV cycles in 1 M KOH solution for HER and OER still maintain the shape of the nanorods, and no obvious change of the surface morphology was found, indicating the outstanding structural stability of Ni–P nanorod electrodes [insert of Figs. 7(c) and 7(d)].

C. The electrocatalytic performance of Ni–P nanorods for overall water splitting

Inspired by the active and stable catalytic activity of the Ni–P catalysts for two half-reactions of water electrolysis in 1.0 M KOH, we believed that it could act as an electrocatalyst for overall water splitting. To illustrate the practical application of the Ni–P sample with two hours of phosphating treatment, the overall water splitting reaction was researched based on a two-electrode setup using Ni–P as both anode and cathode toward OER and HER in a basic environment. A catalytic current was observed when the applied potential was larger than 1.50 V [Fig. 8(a)]. Under the circumstances, a low decomposition voltage of 1.6 V is needed to afford a current density of 10 mA/cm^2 for overall water splitting [Fig. 8(a)]. This potential compares favorably with the reported results, such as C@Ni_8P_3 (1.65 V),[48] Ni–P (1.68 V),[32] Ni_2P (1.6 V),[59] Ni–P (1.69 V),[36] CP @ Ni–P (1.63 V)[22] Ni–P (~1.65 V),[60] as well as commercial electrolyzers (1.8–2.0 V), as shown in Table II.[61] Additionally, the Ni–P sample with two hours of phosphating treatment also exhibited an impressive durability toward the overall water splitting reaction. As demonstrated in Fig. 8(b), the current density can still stabilize at ~10 mA/cm^2 after 12 h of electrolysis when the applied potential is 1.60 V, suggesting their promise to replace precious metal catalysts for the production of clean energy.

IV. CONCLUSIONS

In summary, the biphasic Ni–P nanorods with a rough surface composed of tiny fibers were grown on an acid-treated Ni foam via direct phosphorization of the Ni foam in a tube furnace, where $NaH_2PO_2{\cdot}H_2O$ provided the phosphorous vapor. The time of phosphating treatment has important influence on the electrochemical activity of active materials. The obtained Ni–P sample with two hours of phosphating treatment exhibits enhanced catalytic performance toward both HER and OER in the alkaline solution because of the large active surface area and small charge transfer resistance. Furthermore, a current density of 10 mA/cm^2 can be delivered at a cell voltage of 1.60 V by an efficient water electrolyzer with good stability using the Ni–P 2 h sample as both cathode and anode in an alkaline electrolyte. This work further

underlines the promising application of nickel phosphides for the overall water splitting reaction.

REFERENCES

1. Y. Shi and B. Zhang: Recent advances in transition metal phosphide nanomaterials: Synthesis and applications in hydrogen evolution reaction. *Chem. Soc. Rev.* **45**, 1529–1541 (2016).
2. M.S. Balogun, W. Qiu, Y. Huang, H. Yang, R. Xu, W. Zhao, G. Li, H. Ji, and Y. Tong: Cost-effective alkaline water electrolysis based on nitrogen-and phosphorus-doped self-supportive electrocatalysts. *Adv. Mater.* **29**, 1702095–1702106 (2017).
3. L.G. Bloor, P.I. Molina, M.D. Symes, and L. Cronin: Low pH electrolytic water splitting using earth-abundant metastable catalysts that self-assemble in situ. *J. Am. Chem. Soc.* **136**, 3304–3311 (2014).
4. M.D. Kärkäs, O. Verho, E.V. Johnston, and B. Åkermark: Artificial photosynthesis: Molecular systems for catalytic water oxidation. *Chem. Rev.* **114**, 11863–12001 (2014).
5. Y. Shim, R.M. Young, A.P. Douvalis, S.M. Dyar, B.D. Yuhas, T. Bakas, M.R. Wasielewski, and M.G. Kanatzidis: Enhanced photochemical hydrogen evolution from Fe_4S_4-based biomimetic chalcogels containing M^{2+} (M = Pt, Zn, Co, Ni, Sn) centers. *J. Am. Chem. Soc.* **136**, 13371–13380 (2014).
6. M.S. Balogun, W. Qiu, H. Yang, W. Fan, Y. Huang, P. Fang, G. Li, H. Ji, and Y. Tong: A monolithic metal-free electrocatalyst for oxygen evolution reaction and overall water splitting. *Energy Environ. Sci.* **9**, 3411–3416 (2016).
7. J. Chang, Y. Xiao, M. Xiao, J. Ge, C. Liu, and W. Xing: Surface oxidized cobalt-phosphide nanorods as an advanced oxygen evolution catalyst in alkaline solution. *ACS Catal.* **5**, 6874–6878 (2015).
8. X. Fan, M.S. Balogun, Y. Huang, and Y.X. Tong: Oxygen deficient three-dimensional porous Co_3O_4 nanowires as electrode material for water oxidation and energy storage. *ChemElectroChem*. **29**, 1700607–1700615 (2017).
9. D. Li, H. Baydoun, C.N. Verani, and S.L. Brock: Efficient water oxidation using CoMnP nanoparticles. *J. Am. Chem. Soc.* **138**, 4006–4009 (2016).
10. H. Duan, D. Li, Y. Tang, Y. He, S. Ji, R. Wang, H. Lv, P.P. Lopes, A.P. Paulikas, H. Li, S.X. Mao, C. Wang, N.M. Markovic, J. Li, V.R. Stamenkovic, and Y. Li: High-performance Rh_2P electrocatalyst for efficient water splitting. *J. Am. Chem. Soc.* **139**, 5494–5502 (2017).
11. Y. Lee, J. Suntivich, K.J. May, E.E. Perry, and Y. Shao-Horn: Synthesis and activities of rutile IrO_2 and RuO_2 nanoparticles for oxygen evolution in acid and alkaline solutions. *J. Phys. Chem. Lett.* **3**, 399–404 (2012).
12. X. Long, G. Li, Z. Wang, H. Zhu, T. Zhang, S. Xiao, W. Guo, and S. Yang: Metallic iron-nickel sulfide ultrathin nanosheets as a highly active electrocatalyst for hydrogen evolution reaction in acidic media. *J. Am. Chem. Soc.* **137**, 11900–11903 (2015).
13. B. You and Y. Sun: Hierarchically porous nickel sulfide multifunctional superstructures. *Adv. Energy Mater.* **6**, 1502333 (2016).
14. K. Xu, H. Ding, K.C. Jia, X. Lu, P.Z. Chen, T.P. Zhou, H. Cheng, S. Liu, C.Z. Wu, and Y. Xie: Solution-liquid–solid synthesis of hexagonal nickel selenide nanowire srrays with a nonmetal catalyst. *Angew. Chem., Int. Ed.* **55**, 1710–1713 (2016).
15. F.M. Wang, Y.C. Li, T.A. Shifa, K.L. Liu, F. Wang, Z.X. Wang, P. Xu, Q.S. Wang, and J. He: Selenium-enriched nickel selenide nanosheets as a robust electrocatalyst for hydrogen generation. *Angew. Chem.* **128**, 7033–7038 (2016).
16. K. Xu, H. Ding, H.F. Lv, P.Z. Chen, X.L. Lu, H. Cheng, T.P. Zhou, S. Liu, X.J. Wu, C.Z. Wu, and Y. Xie: Dual electricalbehavior regulation on electrocatalysts realizing enhanced electrochemical water oxidation. *Adv. Mater.* **28**, 3326–3332 (2016).
17. C. Wan and B.M. Leonard: Iron-doped molybdenum carbide catalyst with high activity and stability for the hydrogen evolution reaction. *Chem. Mater.* **27**, 4281–4288 (2015).
18. P.Z. Chen, K. Xu, T.P. Zhou, Y. Tong, J.C. Wu, H. Cheng, X.L. Lu, H. Ding, C.Z. Wu, and Y. Xie: Strong-coupled cobalt borate nanosheets/graphene hybrid as electrocatalyst for water oxidation under both alkaline and neutral conditions. *Angew. Chem., Int. Ed.* **55**, 2488–2492 (2016).
19. W. Liu, L. Zhang, W. Yan, W. Yan, X. Liu, X. Yang, S. Miao, W. Wang, A. Wang, and T. Zhang: Single-atom dispersed Co–N–C catalyst: Structure identification and performance for hydrogenative coupling of nitroarenes. *Chem. Sci.* **7**, 5758–5764 (2016).
20. F. Hu, H. Yang, C. Wang, Y. Zhang, H. Lu, and Q. Wang: Co–N-doped mesoporous carbon hollow spheres as highly efficient electrocatalysts for oxygen reduction reaction. *Small* **13**, 2507–2518 (2017).
21. W. Li, X. Gao, X. Wang, D. Xiong, P. Huang, W. Song, X. Bao, and L. Liu: From water reduction to oxidation: Janus Co–Ni–P nanowires as high-efficiency and ultrastable electrocatalysts for over 3000 h water splitting. *J. Power Sources* **330**, 156–166 (2016).
22. X. Wang, W. Li, D. Xiong, D.Y. Petrovykh, and L. Liu: Bifunctional nickel phosphide nanocatalysts supported on carbon fiber paper for highly efficient and stable overall water splitting. *Adv. Funct. Mater.* **26**, 4067–4077 (2016).
23. X. Wang, Y.V. Kolen'ko, and L. Liu: Direct solvothermal phosphorization of nickel foam to fabricate integrated Ni_2P–nanorods/Ni electrodes for efficient electrocatalytic hydrogen evolution. *Chem. Commun.* **51**, 6738–6741 (2015).
24. F.H. Saadi, A.I. Carim, E. Verlage, J.C. Hemminger, N.S. Lewis, and M.P. Soriaga: CoP as an acid-stable active electrocatalyst for the hydrogen-evolution reaction: Electrochemical synthesis, interfacial characterization and performance evaluation. *J. Phys. Chem. C* **118**, 29294–29300 (2014).
25. X. Yang, A.Y. Lu, Y. Zhu, M.N. Hedhili, S. Min, K. Huang, Y. Han, and L. Li: CoP nanosheet assembly grown on carbon cloth: A highly efficient electrocatalyst for hydrogen generation. *Nano Energy* **15**, 634–641 (2015).
26. Z. Zhang, J. Hao, W. Yang, and J. Tang: Defect-rich CoP/nitrogen-doped carbon composites derived from a metal-organic framework: High-performance electrocatalysts for the hydrogen evolution reaction. *ChemCatChem* **7**, 1920–1925 (2015).
27. P. Jiang, Q. Liu, Y. Liang, J. Tian, A.M. Asiri, and X. Sun: A cost-effective 3D hydrogen evolution cathode with high catalytic activity: FeP nanowire array as the active phase. *Angew. Chem., Int. Ed.* **53**, 12855–12859 (2014).
28. J. Kibsgaard and T.F. Jaramillo: Molybdenum phosphosulfide: An active, acid-stable, earth-abundant catalyst for the hydrogen evolution reaction. *Angew. Chem., Int. Ed.* **53**, 14433–14437 (2014).
29. J.M. McEnaney, J.C. Crompton, J.F. Callejas, E.J. Popczun, C.G. Read, N.S. Lewis, and R.E. Schaak: Electrocatalytic hydrogen evolution using amorphous tungsten phosphide nanoparticles. *Chem. Commun.* **50**, 11026–11028 (2014).
30. E.J. Popczun, J.R. McKone, C.G. Read, A.J. Biacchi, A.M. Wiltrout, N.S. Lewis, and R.E. Schaak: Nanostructured nickel phosphide as an electrocatalyst for the hydrogen evolution reaction. *J. Am. Chem. Soc.* **135**, 9267–9270 (2013).
31. B. You, N. Jiang, M. Sheng, W. Bhushan, and Y. Sun: Hierarchically porous urchin-like Ni_2P superstructures supported on nickel foam as efficient bifunctional electrocatalysts for overall water splitting. *ACS Catal.* **6**, 714–721 (2015).

32. Q. Liu, S. Gu, and C.M. Li: Electrodeposition of nickel–phosphorus nanoparticles film as a Janus electrocatalyst for electro-splitting of water. *J. Power Sources* **299**, 342–346 (2015).
33. L.A. Stern, L. Feng, F. Song, and X. Hu: Ni_2P as a Janus catalyst for water splitting: The oxygen evolution activity of Ni_2P nanoparticles. *Energy Environ. Sci.* **8**, 2347–2351 (2015).
34. X. Wang, Y.V. Kolen'ko, X.Q. Bao, K. Kovnir, and L. Liu: One-step synthesis of self-supported nickel phosphide nanosheet array cathodes for efficient electrocatalytic hydrogen generation. *Angew. Chem., Int. Ed.* **54**, 8188–8192 (2015).
35. J. Xiao, Q. Lv, Y. Zhang, Z. Zhang, and S. Wang: One-step synthesis of nickel phosphide nanowire array supported on nickel foam with enhanced electrocatalytic water splitting performance. *RSC Adv.* **6**, 107859–107864 (2016).
36. G.F. Chen, T.Y. Ma, Z.Q. Liu, N. Li, Y. Su, K. Davey, and S-Z. Qiao: Efficient and stable bifunctional electrocatalysts Ni/Ni_xM_y (M = P, S) for overall water splitting. *Adv. Funct. Mater.* **26**, 3314–3323 (2016).
37. J. Li, J. Li, X. Zhou, W. Gao, Y. Ma, and Y. Qu: Highly efficient and robust nickel phosphides as bifunctional electrocatalysts for overall water-splitting. *ACS Appl. Mater. Interfaces* **8**, 10826–10834 (2016).
38. B. You, N. Jiang, M. Sheng, S. Gul, J. Yano, and Y. Sun: High-performance overall water splitting electrocatalysts derived from cobalt-based metal–organic frameworks. *Chem. Mater.* **27**, 7636–7642 (2015).
39. Y. Li and C. Zhao: Iron-doped nickel phosphate as synergistic electrocatalyst for water oxidation. *Chem. Mater.* **28**, 5659–5666 (2016).
40. M. Ledendecker, S. Krick Calderón, C. Papp, H.P. Steinrîck, M. Antonietti, and M. Shalom: The synthesis of nanostructured Ni_5P_4 films and their use as a non-noble bifunctional electrocatalyst for full water splitting. *Angew. Chem.* **127**, 12538–12542 (2015).
41. S. Duan and R. Wang: $Au/Ni_{12}P_5$ core/shell nanocrystals from bimetallic heterostructures: In situ synthesis, evolution and supercapacitor properties. *NPG Asia Mater.* **6**, 122 (2014).
42. S. Tian, X. Li, A. Wang, R. Prins, Y. Chen, and Y. Hu: Facile preparation of Ni_2P with a sulfur-containing surface layer by low-temperature reduction of $Ni_2P_2S_6$. *Angew. Chem., Int. Ed.* **55**, 4030–4034 (2016).
43. Z. Sun, H. Zheng, J. Li, and P. Du: Extraordinarily efficient photocatalytic hydrogen evolution in water using semiconductor nanorods integrated with crystalline Ni_2P cocatalysts. *Energy Environ. Sci.* **8**, 2668–2676 (2015).
44. K. Zhou, W. Zhou, L. Yang, J. Lu, S. Cheng, W. Mai, Z. Tang, L. Li, and S. Chen: Ultrahigh-performance pseudocapacitor electrodes based on transition metal phosphide nanosheets array via phosphorization: A general and effective approach. *Adv. Funct. Mater.* **25**, 7530–7538 (2015).
45. P. Xiao, W. Chen, and X. Wang: A review of phosphide-based materials for electrocatalytic hydrogen evolution. *Adv. Energy Mater.* **5**, 1500985–1500998 (2015).
46. L. Feng, H. Vrubel, M. Bensimon, and X. Hu: Easily-prepared dinickel phosphide (Ni_2P) nanoparticles as an efficient and robust electrocatalyst for hydrogen evolution. *Phys. Chem. Chem. Phys.* **16**, 5917–5921 (2014).
47. N.S. Alhajri, D.H. Anjum, and K. Takanabe: Molybdenum carbide-carbon nanocomposites synthesized from a reactive template for electrochemical hydrogen evolution. *J. Mater. Chem. A* **2**, 10548–10556 (2014).
48. J. Yu, Q. Li, N. Chen, C.Y. Xu, L. Zhen, J. Wu, and V.P. Dravid: Carbon-coated nickel phosphide nanosheets as efficient dual-electrocatalyst for overall water splitting. *ACS Appl. Mater. Interfaces* **8**, 27850–27858 (2016).
49. M. Liu and J. Li: Cobalt phosphide hollow polyhedron as efficient bifunctional electrocatalysts for the evolution reaction of hydrogen and oxygen. *ACS Appl. Mater. Interfaces* **8**, 2158–2165 (2016).
50. Q. Dong, C. Sun, Z. Dai, X. Zang, and X. Dong: Free-standing NiO@C nanobelt as an efficient catalyst for water splitting. *ChemCatChem* **8**, 3484–3489 (2016).
51. Z. Peng, D. Jia, A.M. Al-Enizi, A.A. Elzatahry, and G. Zheng: From water oxidation to reduction: Homologous Ni–Co based nanowires as complementary water splitting electrocatalysts. *Adv. Energy Mater.* **5**, 1402031–1402038 (2015).
52. M. Shalom, D. Ressnig, X. Yang, G. Clavel, T.P. Fellinger, and M. Antonietti: Nickel nitride as an efficient electrocatalyst for water splitting. *J. Mater. Chem. A* **3**, 8171–8177 (2015).
53. H. Liang, F. Meng, M. Cabán-Acevedo, L. Li, A. Forticaux, L. Xiu, Z. Wang, and S. Jin: Hydrothermal continuous flow synthesis and exfoliation of NiCo layered double hydroxide nanosheets for enhanced oxygen evolution catalysis. *Nano Lett.* **15**, 1421–1427 (2015).
54. W. Xu, Z. Lu, X. Lei, Y. Li, and X. Sun: A hierarchical Ni–Co–O@Ni–Co–S nanoarray as an advanced oxygen evolution reaction electrode. *Phys. Chem. Chem. Phys.* **16**, 20402–20405 (2014).
55. J. Luo, J.H. Im, and M.T. Mayer: Water photolysis at 12.3% efficiency via perovskite photovoltaics and earth-abundant catalysts. *Science* **345**, 1593–1596 (2014).
56. Q. Liu, J. Tian, W. Cui, P. Jiang, N. Cheng, A.M. Asiri, and X. Sun: Carbon nanotubes decorated with CoP nanocrystals: A highly active non-noble-metal nanohybrid electrocatalyst for hydrogen evolution. *Angew. Chem.* **126**, 6828–6832 (2014).
57. N. Zhang, S. Gan, T. Wu, W. Ma, D. Han, and L. Niu: Growth control of MoS_2 nanosheets on carbon cloth for maximum active edges exposed: An excellent hydrogen evolution 3D cathode. *ACS Appl. Mater. Interfaces* **7**, 12193–12202 (2015).
58. A.T. Swesi, J. Masud, and M. Nath: Nickel selenide as a high-efficiency catalyst for oxygen evolution reaction. *Energy Environ. Sci.* **9**, 1771–1782 (2016).
59. X. Wang, W. Li, D. Xiong, and L. Liu: Fast fabrication of self-supported porous nickel phosphide foam for efficient, durable oxygen evolution and overall water splitting. *J. Mater. Chem. A* **4**, 5639–5646 (2016).
60. N. Jiang, B. You, M. Sheng, and Y. Sun: Bifunctionality and mechanism of electrodeposited nickel-phosphorous films for efficient overall water splitting. *ChemCatChem* **8**, 106–112 (2016).
61. K. Zeng and D. Zhang: Recent progress in alkaline water electrolysis for hydrogen production and applications. *Prog. Energy Combust. Sci.* **36**, 307–326 (2010).